

Modeling wildland fire burn severity in California using a spatial Super Learner approach

Nicholas Simafranca¹ · Bryant Willoughby² · Erin O'Neil³ · Sophie Farr⁴ · Brian J. Reich² · Naomi Giertych² · Margaret C. Johnson⁵ · Madeleine A. Pascolini-Campbell⁵

Received: 12 October 2023 / Accepted: 22 January 2024 © The Author(s), under exclusive licence to Springer Science+Business Media, LLC, part of Springer Nature 2024

Abstract

Given the increasing prevalence of wildland fires in the Western US, there is a critical need to develop tools to understand and accurately predict burn severity. We develop a novel machine learning model to predict post-fire burn severity using prefire remotely sensed data. Hydrological, ecological, and topographical variables collected from four regions of California — the site of the Kincade fire (2019), the CZU Lightning Complex fire (2020), the Windy fire (2021), and the KNP Fire (2021) are used as predictors of the differenced normalized burn ratio. We hypothesize that a Super Learner (SL) algorithm that accounts for spatial autocorrelation using Vecchia's Gaussian approximation will accurately model burn severity. We use a crossvalidation study to show that the spatial SL model can predict burn severity with reasonable classification accuracy, including high burn severity events. After fitting and verifying the performance of the SL model, we use interpretable machine learning tools to determine the main drivers of severe burn damage, including greenness, elevation, and fire weather variables. These findings provide actionable insights that enable communities to strategize interventions, such as early fire detection systems, pre-fire season vegetation clearing activities, and resource allocation during emergency responses. When implemented, this model has the potential to minimize the loss of human life, property, resources, and ecosystems in California.

Keywords Ensemble prediction · Kriging · Machine learning · Remote sensing

Handling Editor: Luiz Duczmal.

Simafranca, Willoughby, O'Neil and Farr contributed equally to the paper.

Extended author information available on the last page of the article





1 Introduction

Current trends reveal an increase in the magnitude and frequency of wildland fires in the Western US (Dennison et al. 2014). The rise of "megafires" in recent years posed a threat to the environment, human life, property, and resources (Coen et al. 2018). Wildland fires disturb microclimates by causing "type conversions" of land-scapes (Coop et al. 2020). This is when once dominant vegetation (such as forestry) is replaced with new vegetation (such as grasses). "Type conversions" intensify the conditions conducive to wildland fires by creating a hotter landscape with less moisture (Coop et al. 2020) which also has dangerous social implications. For one, wildland fire smoke has proven to be detrimental to respiratory health (Heaney et al. 2022). Furthermore, communities bear the economic burden of recovering from devastating structural damages. Therefore, studying the factors that influence the severity and spread of burn incidents has reached a critical point. By understanding the drivers of wildland fires, communities can effectively allocate their time and resources to minimize losses.

Burn severity is a metric used to evaluate the post-fire damage to soil and vegetation (Keeley 2009). This metric is influenced by the availability and flammability of fuels, environmental stressors, and topography (Coen et al. 2018). Previous studies have shown that plant water stress variables are important for predicting burn severity (Pascolini-Cambell et al. 2021). There is also evidence that pre-season soil moisture is a strong predictor (Jensen et al. 2018). Data from the ECOsystem and Spaceborne Thermal Radiometer Experiment on Space Station (ECOSTRESS) satellite (Fisher et al. 2020) provides high spatial (70 m) and temporal (3-5 days) resolution of hydrological information such as evapotranspiration (ET), evaporative stress index (ESI), and water use efficiency (WUE). We incorporate these variables into our study due to their relevance in characterizing fuel amount and flammability. We hypothesize that these variables will increase the predictability of burn severity. Regions with greater plant productivity, and more fire fuel, tend to have higher measures of ET (Fisher et al. 2010). Moreover, ESI, which evaluates the moisture available to vegetation, serves as an indicator of the flammability of those fuels (Huang et al. 2020). Finally, WUE measurements provide insight into the vulnerability of plants to climatic stressors (Pascolini-Cambell et al. 2021). The complex relationship between fuels, climate and topography influences the spatial patterns of burn severity (Kane et al. 2015a). Due to this complexity, the prediction of the spatial patterns of burn severity has garnered the attention of researchers in recent decades.

Traditional physics-based simulations that capture physical processes (Hoffman et al. 2015) pose challenges. These simulators are time dependent and rely on numerical solutions to computational fluid dynamics. Jain et al. (2020) reports that it is unfeasible to apply such models on large scales and often produce low accuracy. To overcome these issues, many wildland fire researchers turn to empirical and statistical models. However, this requires the implementation of nonlinear relationships, introducing complexity. Machine learning (ML) has emerged as a contemporary approach in wildland fire research. This approach is independent of the



implementation of physical processes. Instead, it learns directly from data (Jain et al. 2020). Many ML methods, henceforth referred to as base learners, have been applied to wildland fire prediction including Random Forests (RF), MaxEnt, Artificial Neural Networks, Decision Trees, Support Vector Machines (SVM), and Genetic Algorithms (Jain et al. 2020).

A study of the Basic Complex fire (2008) in Big-Sur, California compared the performance of RF, Gaussian Process Regression (GPR), and SVM to multiple regression in assessing burn severity. RF performed the best and reduced model error by 48% compared to Linear Regression. This reduction in model error is likely due to its ensemble learning approach (Hultquist et al. 2014). Ensemble learning merges multiple base learners to solve a single learning problem (Zhou 2021). To date, the use of ensemble ML models to predict burn severity remains relatively unexplored. Current literature indicates that ensemble learning outperforms individual learners (e.g., van Breugel et al. 2015). When base algorithms are accurate and diverse, performance is further enhanced (Zhou 2021). Our model incorporates a Super Learner ensemble algorithm that aggregates diverse base learners by stacking them in a second-stage regression (van der Laan et al. 2007) to forecast wildland burn severity. In addition, our model accounts for spatial autocorrelation both in estimating the stacking weights and regression residuals. To the best of our knowledge, this has yet to be done for burn severity.

Our motivation for combining ensemble prediction and spatial modeling stems from current literature which reveals the effectiveness of combining ML algorithms with traditional spatial statistics methods. When handling spatially dependent data, ML algorithms alone are limited in their ability to account for common errors that arise in geostatistics such as data gaps (Wikle and Zammit-Mangion 2023). Furthermore, unlike geostatistical methods, many common machine learning algorithms are not able to provide estimates of prediction or classification error (Wikle and Zammit-Mangion 2023).

Applying a ML algorithm in conjunction with a statistical method is likely to be more applicable to spatially correlated data and yield stronger predictions. There are multiple ways to implement a spatial-ML model; one way is to account for spatial correlation after implementing the ML algorithm (Fayad et al. 2016). Another is attempting to account for spatial correlation within the ML algorithm, such as Random Forest (Hengl et al. 2018). Li et al. (2011) found that a combination of Random Forest and Ordinary Kriging (a form of spatial prediction) provided the best results out of 23 methods. Current literature reveals that spatial prediction is used in tandem with diverse ML algorithms. Koike et al. (2001) got the most accurate predictions at new locations after training with a Multi-layer Neural Network that includes spatial relationships compared to just ordinal Kriging and normal Multi-layer Neural Network. Another paper also found the benefits of combining Neural Networks and Kriging for spatial prediction (Yasrebi et al. 2020).

A mixed spatial ML model was proposed by Saha et al. (2021) that incorporates a RF machine learning algorithm and accounts for spatial autocorrelation using Gaussian processes. The mixed-model approach proved superior to RF alone when evaluating spatially correlated data. Davies and van der Laan (2016) examine the use of an ensemble machine learning algorithm that includes Kriging in its base learner



library. The favorabilty of a mixed-method approach was further confirmed by their results which found that SL performs as good or better than the best base learner in spatial prediction. Similarly, Kim (2022) takes a Bayesian approach to average over uncertainty in the form of regression trees to improve spatial prediction. Another study found that optimizing the predictions from both Kriging and SL separately provided an accurate estimation of geological attributes (Gamze Erdogan Erten 2022). Because there is strong geospatial correlation in our wildland fire datasets, we expect to find that accounting for spatial correlation on the ensemble predictions will enhance the prediction performance of our SL model.

In this study, we investigate the spatial pattern of burn severity of four wildfires between 2019-2021. Two fires, the Kincade and San Mateo–Santa Cruz Unit (CZU) Lightning Complex fire, represent fires occurring along the Northern Pacific Coast in California (California Department of Forestry and Fire Protection 2023). This territory is characterized by a warm/hot summer Mediterranean climate. In contrast, the Windy and Sequoia and Kings Canyon National Park (KNP) Complex represents fires that occur in the Sierra Nevada region which spans the majority of the inland mid-latitudes of California (InciWeb 2022). A dry summer subarctic climate can be found in this region. This paper is motivated by the questions:

- How can we relate areas of intense burn to vegetation, weather, and topography?
- Can a Super Learner algorithm accurately predict post-wildfire burn severity throughout California?
- Which variables are most important to burn severity?

The remainder of the paper proceeds as follows. The wildland fire data are described in Sect. 2. Section 3 introduces the methods and computational algorithms. The results are summarized in Sect. 4. Section 5 concludes.

2 Data description

We analyze data from four fires in California: the Kincade fire, the CZU Lightning Complex fire, the Windy fire, and the KNP Fire. The fires are described in Table 1 and plotted in Fig. 1. The data sources described in this section include the ECOSTRESS satellite (Hook and Hulley 2019c, a, b, d), Harmonized Landsat Sentinel (Masek et al. 2021b, a), Digital Elevation Model (NASA JPL 2013), Moderate

Table 1 Summary of wildland fires used in the study. Images are captured pre-fire onset within a two week time interval

Fire	Location	Ignited	Fully contained	Acreage	# of Pixels
Kincade	Sonoma County, CA	Oct. 23, 2019	Nov. 6, 2019	77,758	82,125
CZU	Santa Cruz & San Mateo, CA	Aug. 16, 2020	Sept. 22, 2020	86,509	88,581
Windy	Sierra Nevada, CA	Sept. 9, 2021	Nov. 15, 2021	97,528	99,458
KNP	Sierra Nevada, CA	Sept. 9, 2021	Dec. 16, 2021	88,307	92,171



Table 2 Variables used as covariates in the Super Learner model

Variable	Source	Resolution
Evapotranspiration (ET)	ECOSTRESS	70 m
Evaportaive stress index (ESI)	ECOSTRESS	70 m
Water use efficiency (WUE)	ECOSTRESS	70 m
Land surface temperature (LST)	ECOSTRESS	70 m
Normalized differened vegetation index (NDVI)	Harmonized Landsat Sentinel	30 m
Leaf area index (LAI)	MODIS	500 m
AM soil moisture (AM SM)	SMAP	9 km
PM soil moisture (PM SM)	SMAP	9 km
Daily average dew point temperature (TDMEAN)	PRISM	4 km
Daily average air temperature (TMEAN)	PRISM	4 km
Vapor pressure deficit maximum (VPDMAX)	PRISM	4 km
Vapor pressure deficit minimum (VPDMIN)	PRISM	4 km
Elevation	Digital Elevation Model	30 m
Aspect	Digital Elevation Model	30 m
Slope	Digital Elevation Model	30 m

These the exception of the final three variables, all variable were included as both their current state and temporal trend

Table 3 Number of satellite images in the two weeks prior to the onset of the fire for each fire (Table 1) and covariate (Table 2); the covariates TDMEAN, TMEAN, VPDMAX and VPDMIN all have at least 14 images for each fire

Fire	LST	ET	ESI	WUE	LAI	NDVI	AM SM	PM SM
Kincade	4	4	4	4	4	6	8	6
CZU	7	6	7	7	5	4	7	8
Windy	10	3	3	3	4	6	6	7
KNP	12	4	4	4	6	8	6	7

Resolution Imaging Spectroradiometer (Friedl and Sulla-Menashe 2022, MODIS), Parameter-elevation Relationships on Independent Slopes Model (PRISM Climate Group 2023), and Soil Moisture Active Passive (SMAP 2023) (Table 2). All products were regridded to 70 m resolution to match the resolution of the ECOSTRESS data. The burn severity response variable (Sect. 2.1) is obtained after the fire, and thus is observed only once per pixel per fire. The predictor variables (Sects. 2.2) are all measured before the onset of the fire and some are measured multiple times in the two weeks prior to the onset of the fire. For instance, for the KNP fire, the Water Use Efficiency (WUE) variable was measured four times before the onset of ignition (Aug. 26, Aug. 30, Sep. 03, and Sep. 07). For each of the four fires, the number of pre-fire images captured for each covariate (defined in Table 2) is summarized in Table 3. In Sect. 2.3 we describe how we handle missing data and how we resolve the repeated measures.



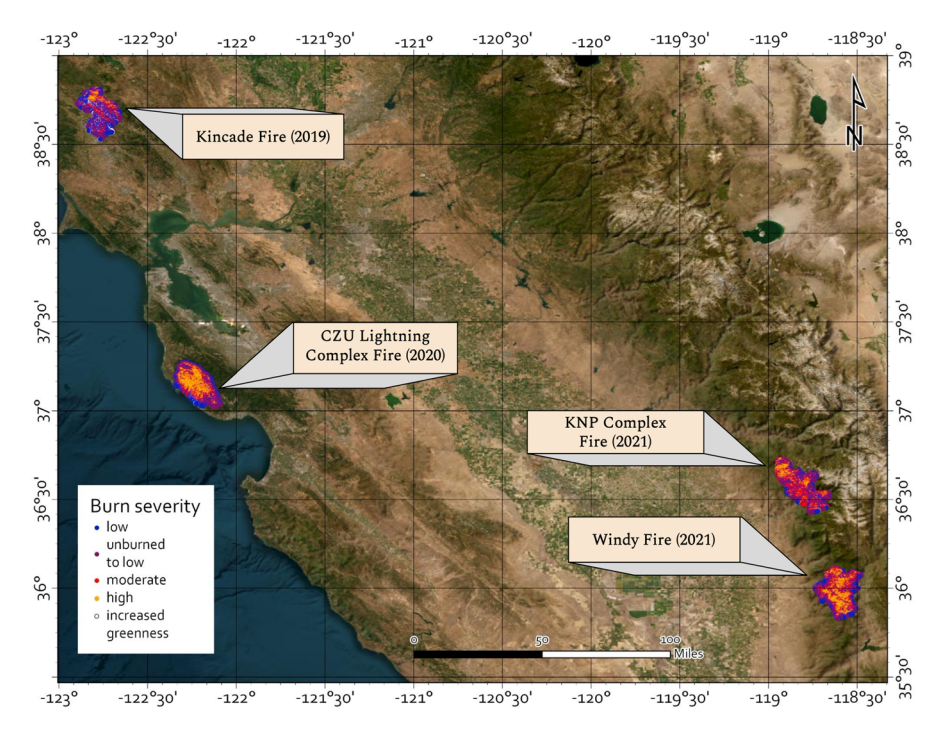


Fig. 1 Maps of the burn severity measure (dNBR) for the Californian wildland fires described in Table 1

2.1 Burn severity

Our outcome variable of interest is burn severity, which is a function of the normalized burn ratio (NBR). NBR compares measurements in the near infrared (NIR) and the short-wave infrared (SWIR) sections of the electromagnetic spectrum as

$$NBR = \frac{NIR - SWIR}{NIR + SWIR}. (1)$$

Healthy vegetation reflects in the NIR section whereas burned vegetation reflects stronger in the SWIR section (Pascolini-Cambell et al. 2021). The response variable is the differenced normalized burn ratio, or dNBR, which is the difference between pre-fire NBR and post-fire NBR so that a large dNBR value implies extreme burn severity and vice versa. Landsat 30 m images were used to calculate dNBR values. The dNBR data was retrieved from the interagency program "Monitoring Trends in Burn Severity (MTBS)" and multiplied by 1,000. We change this continuous measure of burn severity to a categorical measure using the following categories Wasser (2019): high enhanced growth (dNBR from – 500 to – 251), low enhanced regrowth (– 250 to – 101), unburned (– 100 –99), low (100 –269), moderate-low (270 –439), moderate-high (440 –659), and high (660–1300). We build our model



for the continuous severity response, but evaluate performance for correctly predicting the categorical measure.

2.2 Covariates

Data for each covariate was collected within a two-week period preceding fire onset. We are interested in a snap shot of conditions before the fire which gives different information to longer-term information. The snapshot will capture week-to-week variability in fire weather and plant stress conditions conducive to extreme fire conditions, whereas longer term would capture more slowly varying drought and climate processes. For this study we are interested in short-term drivers. Using a two week pre-fire time interval ensures our predictions are based on relevant pre-fire conditions while still providing a sufficient amount of data. We acquired variables at a 70 m resolution describing plant water stress from the ECOSTRESS (Fisher et al. 2020), which gives information on fuel availability, drought, and other potentially important predictors of wildland fire burn severity (Pascolini-Cambell et al. 2021). Evapotranspiration (ET) measures the amount of water being lost in the soil from both evaporation from soil surface and transpiration from the plant leaves. The Evaportaive Stress Index (ESI) is the ratio of actual ET to potential ET, and can be an indicator of drought. Water use efficiency (WUE) indicates how a plant responds to stress, such as short-term drought. Land surface temperature (LST) is defined as the temperature that the land would feel to the touch.

In addition to ECOSTRESS measurements, we include variables describing vegetation. The normalized differenced vegetation index (NDVI) and the leaf area index (LAI) quantify the plant canopies. The morning soil moisture (AM SM) and afternoon soil moisture (PM SM) were also variables of interest. Moreover, we have variables describing weather two weeks before the fire. These include both morning and evening soil moisture, daily average dew point temperature (TDMEAN), daily average air temperature (TMEAN), vapor pressure maximum (VPDMAX), and vapor pressure minimum (VPDMIN). Lastly, the variables elevation, slope, and aspect, describe the topography of the region. A summary of the covariates with their corresponding satellite origin and original product resolutions are provided in Table 2.

2.3 Data manipulation

The variables used in the study are derived from different sources and thus have different spatial resolutions (Table 2). The resolution differences are resolved by converting all variables to the ECOSTRESS 70 m grid using area-weighted averaging. We used bilinear interpolation for continuous variables and nearest neighbor for categorical variables using the raster package in R (Hijmans 2023). Missing data is present due to factors such as cloud coverage. We removed variables with more than 28% missing pixels across each geographic region. For the remaining variables, missing observations were imputed using KNearest Neighbor imputation, with K=10 and distance defined using latitude and longitude.



Many of the variables are collected at different times within the two-week period leading up to the fire ignition. To resolve collinearity between subsequent measurements and harmonize variables across fires with a different number of replications of the variables, we convert the sequence of observations to estimates of the current value and the trend at the time of ignition for each pixel. Variables that are treated in this way will be labeled with the term "current" or "trend." For instance, TDMEAN (trend) would refer to the change in average dew point temperature over the time interval of our data and TDMEAN (current) would refer to the average dew point temperature at the onset of the fire. Estimates are made using Linear Regression separately by variable and pixel. For example, let ET_{it} be the observed evapotranspiration (ET) at spatial location \mathbf{s}_i t days before ignition. We then fit the linear model $\mathbf{E}(ET_{it}) = \beta_{0i} + \beta_{1i}t$ and use the least-squares estimates of β_{0i} and β_{1i} as covariates to summarize the current value and trend in ET, respectively, for pixel i at the time of ignition. Therefore, even the variables labelled as "current" are functions of observations made prior to ignition.

3 Statistical methods

In this section, we discuss the methods used for predicting the continuous burn severity response variable; the method is summarized in Fig. 2. We implement a spatial extension of a SL algorithm, an ensemble learning method that combines base learners to achieve superior predictive accuracy. Section 3.1 gives the overall model framework. The model is fit in two stages: in the first stage (Sect. 3.2) we use non-spatial regression to train the base learners and in the second stage (Sect. 3.3) we use the first-stage estimates as covariates and fit a spatial process model used for prediction (Sect. 3.4).

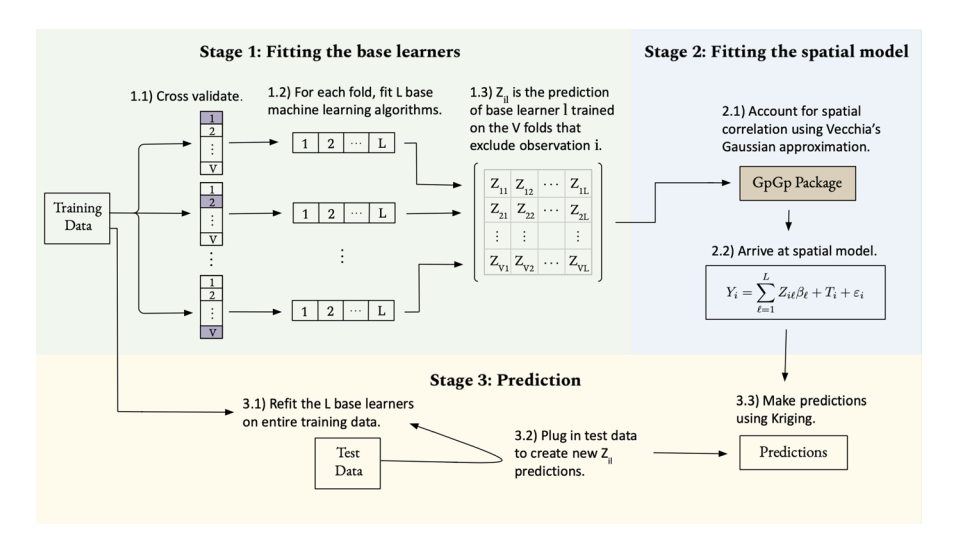


Fig. 2 Flowchart depicting the Super Learner algorithm (based on a diagram from van der Laan et al. (2007))



3.1 Spatial Super Learner model

Let Y_i be the continuous measure of burn severity (dNBR) at spatial location \mathbf{s}_i , and $\mathbf{X}_i = (X_{i1},...,X_{ip})$ be the associated covariates (the p=27 variables in Table 2). Rather than using the covariates directly in the linear model, we use them to train L machine learning algorithms (e.g., RF) to allow for interactions and non-linearity, and use the outputs of these algorithms as predictors in the next stage. Denote $Z_{il} = f_l(\mathbf{X}_i)$ as the non-linear function of the covariates determined by learner $l \in \{1,...,L\}$. The spatial model is

$$Y_i = \beta_0 + \sum_{l=1}^{L} Z_{il} \beta_l + T_i + \varepsilon_i, \qquad (2)$$

where β_0 is the intercept, β_l is the weight given to learner l, T_i is the spatially-correlated error and ε_i^{iid} Normal $(0,\tau^2)$ is an independent error that accounts for small-scale, unexplained variance. The spatial error term T_i captures correlation not explained by the covariates and is taken to be a stationary Gaussian process with $\mathrm{E}\left(T_i\right)=0$, $\mathrm{Var}\left(T_i\right)=\sigma^2$ and isotropic exponential correlation function $\mathrm{Cor}\left(T_i,T_j\right)=\exp(-d_{ij}/\phi)$, with d_{ij} denoting the distance between \mathbf{s}_i and \mathbf{s}_j , while ϕ is the spatial range parameter.

3.2 Stage 1: fitting the base learners

The Super Learner is a stacking ensemble method, introduced by van der Laan et al. (2007), that seeks the optimal combination of base learners ensuring predictive performance at least as well or better than the best performing base learner. The effectiveness of SL is attributed to the diversity of its base learners. Different learners, each offering a unique approach to problem solving, contribute to a robust and adaptive model. The choice of base learners can be customized based on the requirements or constraints of a given problem. We incorporate L=11 diverse base learners: Elastic Net (Zou and Hastie 2005), Decision Tree Regression (Morgan and Sonquist 1963), Ridge Regression (Hoerl and Kennard 1970b, a), Lasso Regression (Tibshirani 1996), KNearest Neighbors Regression (Cover and Hart 1967), Gradient Boosting Regression (Friedman 2001), XGBoost Regression (Chen and Guestrin 2016), Bagging Regression (Breiman 1996), Random Forest Regression (Breiman 2001), Extra Trees Regression (Geurts et al. 2006), and Multilayered Perceptron Regression (Rosenblatt 1958). The first 10 base learners in the aforementioned list were implemented using the scikit-learn package (Pedregosa et al. 2011).

The base learners are fit individually and without regard to spatial correlation. For model-fitting (we take a slightly different approach for prediction in Sect. 3.4), the training data are split into 10 folds using completely random sampling over i. The covariate Z_{il} in (2) is the prediction of base learner l trained on the 9 folds that exclude observation i. Cross validating tests our models ability to perform well on unseen data and prevents possible overfitting. This method of cross validation was implemented for



both the within-fire (those predictions from which the training and test data are from the same fire) and combined fire datasets (those predictions from which the training data is derived of multiple fires and tested on a subset of that data). More details of base learner training are given in Appendix A.1.

3.3 Stage 2: fitting the spatial model

For the purpose of estimating the parameters $\{\beta_0,...,\beta_p,\sigma^2,\tau^2,\phi\}$ in (2), we treat the base learner predictions Z_{il} as fixed and known covariates and fit a standard spatial linear regression model. Unlike some SL estimators (van der Laan et al. 2007), we do not restrict the weights $\beta_1,...,\beta_L$ to be positive or sum to zero. Since we fit the base learners under a working assumption of independent residuals, we allow for the possibility that their relationship with the response may change considerably when spatial dependence is included (e.g., Hodges and Reich 2010). Therefore, we estimate the weights using unconstrained (i.e., without a sum-to-zero constraint) spatial regression to compensate for fitting the base learners using non-spatial regression. The regression coefficients β_l are identifiable in the two-stage approach if the first-stage estimates of the Z_{il} are linearly-independent.

Due to the large number of pixels (Table 1), the exact maximum likelihood estimator cannot be computed and so we use the Vecchia approximation (Vecchia 1988) implemented in the GpGp package (Guinness et al. 2021). The Vecchia approximation orders the observations and approximates the joint likelihood as a product of the univariate conditional distributions of each site given a local subset of sites that appear before the site in the ordering. In our analysis, we use the default number of nearby sites in the subset (k = 15) and ordering scheme.

3.4 Stage 3: Prediction

For prediction on the training data, we refit the base learners using the entire training dataset and compute fitted values at the training locations and predicted values at the testing locations as the covariates, Z_{il} (Fig. 2). Given these covariates, standard Kriging predictions can be applied. For prediction, we use the estimated parameters (including the β_l) from the Stage-2 spatial regression fit. However, due to the size of the training data, standard methods are too computationally expensive and so we use the local Kriging prediction option in the GpGp package that makes predictions at a test location based on the nearest k training set observations. Given the predicted values for the continuous measure of burn severity, we predict the categorical burn severity measure by discretizing the Kriging prediction into the corresponding category using the thresholds given in Sect. 2.1. Details of fitting the spatial model and subsequent prediction are given in Appendix A.2.



4 Results

4.1 Within-fire predictions

We first analyze the four fires separately. We fit four models (Table 4): Linear Regression versus SL for the mean with spatial versus independent errors. The first step in the spatial SL method is to compute the base-learner predictions, Z_{ii} . Table 5 gives the sample correlations between the base learners for the KNP fire. The base learners with the largest β_l contribute the most to the predictive model. While there are some highly correlated base learners, there are many with moderate correlation and so as desired the set of base learners is diverse and conducive to ensemble prediction. Table 6 gives estimates of the weight parameters, β_l , for the spatial SL fit for each fire. For all fires, extra trees regression has the most weight followed by multilayer perceptron regression and XGBoost regression. The consistency of the β_l estimates across fires and small standard errors suggest the model weights are well identified. We did not restrict the mean of the spatial model to be a convex combination of the base learners because the base learners were fit under independence. However, the intercept estimates are all near zero and the weights are mostly positive or near zero and sum to approximately one for each fire. The consistency of the results across fires also suggests the predictive model may be generalizable across similar fires.

Methods are compared in Table 7 using prediction Root Mean Squared Error (RMSE), classification accuracy for all categories, and classification accuracy for high burn severity categories. For all four fires, the non-spatial linear regression models perform poorly with high RMSE and low classification accuracy. Including either the SL model in the mean or spatial dependence gives a large reduction in MSE and an increase in classification accuracy. Across the four fires, the classification accuracy of the spatial SL approach for predicting the burn severity category is between 58 and 71%, and thus the predictions are fairly reliable.

Table 4 Spatial-coordinates only (S), linear regression (LR) and Super Learner (SL) models for the mean with spatial versus independent errors for $p \in \{1, ..., P\}$ covariates and $l \in \{1, ..., L\}$ base learners

Mean	Covariance	Model
S	Independent	$Y_i = \beta_0 + s_{i1}\beta_1 + s_{i2}\beta_2 + \varepsilon_i$
S	Spatial	$Y_i = \beta_0 + s_{i1}\beta_1 + s_{i2}\beta_2 + T_i + \varepsilon_i$
LR	Independent	$Y_i = \beta_0 + \sum_{p=1}^{P} X_{ip} \beta_p + \varepsilon_i$
LR	Spatial	$Y_i = \beta_0 + \sum_{p=1}^{P} X_{ip} \beta_p + T_i + \varepsilon_i$
SL	Independent	$Y_i = \beta_0 + \sum_{l=1}^{L} Z_{il} \beta_l + \varepsilon_i$
SL	Spatial	$Y_i = \beta_0 + \sum_{l=1}^{L} Z_{il} \beta_l + T_i + \varepsilon_i$

The mean models differ by whether spatial coordinates ($\mathbf{s}_i = (s_{i1}, s_{i2})$), the original covariates (X_{ip}) or the base learners (Z_{il}) are included in the mean and whether the spatial random effects (T_i) are included in the covariance



Table 5 Correlations between the base learners for the KNP fire

	Decision tree	Ridge reg	Lasso reg	tree Ridge reg Lasso reg KNeighbors Reg Gradient boosting reg	Gradient boosting reg	XGBoost reg	XGBoost reg Bagging reg Random forest reg	Random forest reg	Extra trees reg Multilayered perceptron reg	Multilayered perceptron reg
Elastic Net	0.39	98.0	0.94	0.48	0.50	0.46	0.49	0.49	0.48	0.47
Decision Tree		0.44	0.43	0.74	0.79	0.82	0.82	0.82	0.81	0.74
Ridge Reg			96.0	0.55	0.58	0.54	0.56	0.56	0.55	0.55
Lasso Reg				0.53	0.55	0.51	0.54	0.54	0.53	0.52
KNeighbors Reg					0.90	0.89	0.91	0.91	0.92	0.86
Gradient Boosting Reg						0.95	0.97	0.97	0.86	0.90
XGBoost Reg							0.97	0.97	0.97	0.89
Bagging Reg								0.99	0.98	0.91
Random Forest Reg									0.98	0.91
Extra Trees										0.91



Table 6 Fitted values (standard errors), separate by fire, for the regression coefficients β_i

Parameter	KNP	Windy	CZU	Kincade
Intercept	-0.39 (3.62)	1.65 (4.58)	-1.80 (2.90)	3.67 (1.39)
Elastic net	-0.08 (0.03)	-0.09 (0.03)	-0.05 (0.01)	-0.06 (0.02)
Decision Tree	2e-3 (4e-3)	- 2e-3 (3e-3)	4e-3 (4e-3)	- 2e-4 (4e-3)
Ridge Reg	-0.02 (0.03)	0.05 (0.04)	-0.11 (0.03)	0.04 (0.02)
Lasso Reg	0.05 (0.04)	-0.02 (0.05)	0.14 (0.03)	- 8e-3 (0.03)
KNeighbors Reg	-0.05 (7e-3)	-0.03 (6e-3)	-0.04 (7e-3)	0.03 (7e-3)
Gradient Boosting Reg	0.10 (0.01)	0.13 (0.01)	2e-3 (0.01)	0.16 (0.01)
XGBoost Reg	0.10 (0.01)	0.08 (0.01)	0.17 (0.01)	0.07 (0.01)
Bagging Reg	0.01 (0.03)	-0.03 (0.02)	-0.08 (0.02)	1e-3 (0.03)
Random Forest Reg	0.02 (0.03)	- 1e-3 (0.02)	-0.12 (0.02)	-0.02 (0.03)
Extra Trees Reg	0.56 (0.02)	0.60 (0.01)	0.94 (0.01)	0.49 (0.02)
Multilayered Perceptron Reg	0.29 (7e-3)	0.20 (7e-3)	0.18 (6e-3)	0.29 (7e-3)

Table 7 Within-fire crossvalidation root mean squared prediction error (RMSE), classification accuracy (CA) percent for fire severity level (high enhanced growth (dNBR from - 500 to - 251), low enhanced regrowth (- 250 to - 101), unburned (- 100 - 99), low (100-269), moderate-low (270 - 439), moderate-high (440 -659), and high (660 - 1300)) and CA for the high categories for spatial-coordinates only (S), linear regression (LR) and Super Learner (SL) models with independent and spatial error structure

Fire	Mean	Covariance	RMSE	CA	CA-High
KNP	S	Independent	233	24.0	0.00
	S	Spatial	117	56.9	57.2
	LR	Independent	213	28.0	0.03
	LR	Spatial	115	57.5	57.9
	SL	Independent	121	55.7	53.6
	SL	Spatial	114	58.0	55.4
Windy	S	Independent	259	23.3	0.0
	S	Spatial	104	64.1	75.4
	LR	Independent	215	32.1	9.8
	LR	Spatial	98	66.0	78.1
	SL	Independent	112	61.6	73.2
	SL	Spatial	98	66.5	77.8
CZU	S	Independent	285	19.4	0.0
	S	Spatial	96	68.8	83.5
	LR	Independent	207	37.3	39.0
	LR	Spatial	89	70.1	84.8
	SL	Independent	95	69.3	84.8
	SL	Spatial	91	70.7	86.3
Kincade	S	Independent	232	27.6	0.0
	S	Spatial	98	65.3	63.3
	LR	Independent	164	43.0	17.5
	LR	Spatial	88	66.8	67.8
	SL	Independent	94	65.3	69.1
	SL	Spatial	82	69.3	73.8



Table 8 Fitted values (standard errors), combining all fires, for the regression coefficients β_i

Parameter	Combined
Intercept	-2.37 (1.46)
Elastic Net	-0.01 (0.01)
Decision Tree	-2e-3 (2e-3)
Ridge Reg	6e-3 (0.01)
Lasso Reg	-0.02 (0.01)
K Neighbors Reg	-0.01 (3e-3)
Gradient Boosting Reg	0.08 (6e-3)
XGBoost Reg	0.16 (6e-3)
Bagging Reg	0.03 (0.01)
Random Forest Reg	0.04 (0.01)
Extra Trees Reg	0.63 (8e-3)
Multilayered Perceptron Reg	0.12 (4e-3)

Table 9 Combined-fire cross-validation root mean squared prediction error (RMSE), classification accuracy (CA) percent for fire severity level (*high enhanced growth (dNBR from -500 - -251)*, *low enhanced regrowth (-250 - -101)*, *unburned (-100 - 99)*, *low (100 - 269)*, *moderate-low (270 - 439)*, *moderate-high (440 - 659)*, *and high (660 - 1300)*) and CA for the high categories for linear regression (LR) and Super Learner (SL) models with independent and spatial error structure

Fire	Mean	Covariance	RMSE	CA	CA-High
Combined	LR	Independent	223	29.0	8.26
	LR	Spatial	100	64.5	76.54
	SL	Independent	108	62.4	59.06
	SL	Spatial	97	65.7	62.98

4.2 Combined-fire predictions

In contrast to within-fire predictions, combined-fire predictions combine data from multiple individual fires into one dataset to form predictions. By combining the fires, we can identify how well the model fits differ across the entire region in California that these fires span. The fitted values of the parameters from the spatial SL method in Table 8 again show that extra trees regression is the dominant learner, followed by multilayer perceptron regression and XGBoost regression. Methods are compared in Table 9. The spatial SL model has the lowest RMSE and highest overall classification accuracy, followed closely by the spatial linear regression model, which gives the highest overall classification accuracy for the high category.



4.3 Variable importance measures

While the spatial SL method provides solid prediction performance, it does not inherently provide measures of the effect of individual covariates, which is one of our main objectives. Therefore, in this section we use interpretable machine learning tools to isolate the contribution of individual predictors on burn severity. Due to the high performance of the Extra Trees and XGBoost Regressors at low computational cost, we opted to analyze variable importance using these models. A fitted attribute within the scikit-learnn Python package (Pedregosa et al. 2011) allowed us to extract the strongest predictors of wildland fire burn severity in California. The strongest predictors were calculated using Permutation Feature Importance (PFI). The PFI algorithm ranks the importance of covariates as follows. First, a covariate column is selected within the dataset and its entries are shuffled 10 times. Then, the Extra Trees model is refit with the corrupted covariate column. Finally, a metric of importance is determined by evaluating the reduction of model score with the corrupted column, i.e. if shuffling PM SM resulted in a great reduction in model score, then that would indicate that the afternoon soil moisture is important for predicting burn severity in a given region. This VI measure quantifies the importance of covariates to the mean function, but does not consider spatial correlation (which is an important caveat given the expected spatial dependence Kane et al. (2015b)). This process is repeated for each covariate of interest to determine a ranking.

The top five strongest predictors for each individual fire for Extra Trees and XGBoost are reported in Table 10. The leading predictors for within-fire prediction included the daily average dew point temperature (TDMEAN), normalized differenced vegetation index (NDVI), elevation of topography (Elevation),

Table 10 Variable important (VI) measures for the Extra Trees learner and XGBoost learner on the four separate fires

KNP	VI	Windy	VI	CZU	VI	Kincade	VI
(a) Extra trees							
TDMEAN (trend)	0.23	NDVI (current)	0.33	PM SM (current)	0.38	NDVI (current)	0.54
NDVI (current)	0.19	Elevation	0.17	Elevation	0.24	Elevation	0.15
Elevation	0.14	PM SM (trend)	0.11	NDVI (current)	0.08	AM SM (trend)	0.07
PM SM (trend)	0.10	PM SM (current)	0.08	TDMEAN (current)	0.07	VPDMAX (current)	0.04
AM SM (trend)	0.07	TDMEAN (current)	0.07	TMEAN (trend)	0.07	PM SM (trend)	0.04
(b) XGBoost							
TDMEAN (trend)	0.41	NDVI (current)	0.39	PM SM (current)	0.44	NDVI (current)	0.58
Elevation	0.29	Elevation	0.29	Elevation	0.35	Elevation	0.31
NDVI (current)	0.25	VPDMIN	0.20	ET (trend)	0.14	AM SM (trend)	0.19
PM SM (trend)	0.15	PM SM (trend)	0.17	ESI (trend)	0.13	TDMEAN (trend)	0.11
AM SM (trend)	0.08	PM SM (current)	0.14	VPDMIN (trend)	0.11	PM SM (current)	0.10



afternoon soil moisture (PM SM), morning soil moisture (AM SM), daily average air temperature (TMEAN), and vapor pressure maximum (VPDMAX).

The ranking of variable importance is similar for the combined analysis. Within Extra trees, the five most important variables are NDVI (current) (VI = 0.34), elevation (0.20), PM SM (current) (0.20), LST (current) (0.10) and PM SM (trend) (0.08). Within XGBoost, the five most important variables are NDVI (current) (VI = 0.40), elevation (VI = 0.35), TDMEAN (trend) (VI = 0.20), PM SM (trend) (VI = 0.15), and PM SM (current) (VI = 0.12). In addition to ranking variables based on importance, Fig. 3 plots estimates of the direction of the effects of these covariates to illustrate their relationship with burn severity. The effects are estimated using the Accumulated Local Effects (ALE) of Okoli (2023). The local effect of a covariate is estimated by conditioning on all other covariates and computing the mean burn severity as estimated by the fitted SL model as a function of the covariate. These local estimates are then averaged over the distribution of the other covariates. The covariates with most variability in their ALE are plotted in Fig. 3. These plots suggest that the regions that are the most susceptible to burn damage are those with high greenness (NDVI, current), increasing temperature (TMEAN, trend), high elevation, decreasing vapor pressure definite maximum (VPDMAX, trend), low dew point temperature (TDMEAN, current) and increasing vapor pressure deficit minimum (VPDMIN, trend).

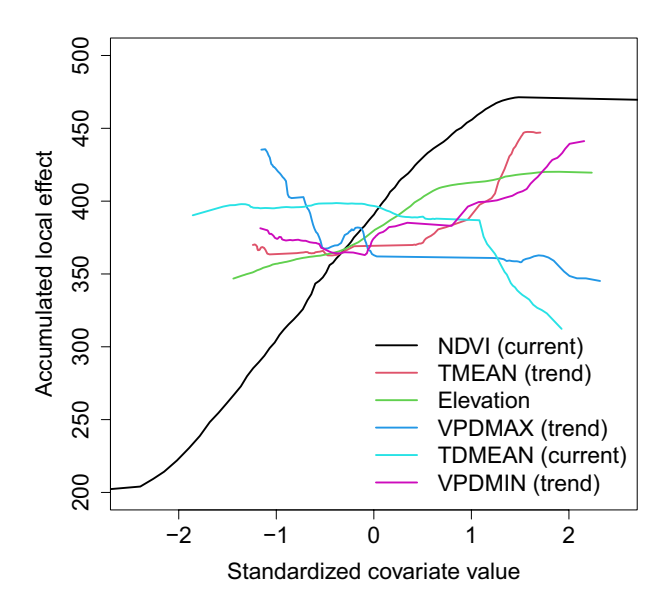


Fig. 3 Accumulated local effects of the most important predictors



5 Discussion

This paper presents the results of evaluating the post-fire burn severity of four California wildfires between 2019-2021 using Super Learner regression and geostatistical techniques designed to handle large and complex datasets. Although computationally expensive, the SL algorithm outperformed all base learners. This result is consistent with papers that have shown that ensemble learning reliably provides a more robust, accurate model than traditional machine algorithms alone. We built upon the work of Pascolini-Campbell et al. by including additional metrics to evaluate burn severity, such as those derived from the SMAP satellite. For the selected fires, hydrological data from ECOSTRESS proved less important than AM soil moisture as the leading predictor of burn severity. This aligns with Jensen et al. (2018) findings of the importance of preseason soil moisture as a strong predictor. Future work could explore the importance of elevation, NDVI, and PM soil moisture for wildland fire prediction.

The current analysis has several limitations. As is often the case with machine learning methods, quantifying prediction uncertainty is not straightforward for the spatial Super Learner algorithm. The prediction variances from GpGp account for uncertainty in the model weights (β_l) and the Kriging variance; they do not account for uncertainty in the first-stage base learner fits (Z_{il}) . Fully characterizing prediction uncertainty is an important area of future work. The approach to manipulating covariate data collected prior to ignition (Sect. 2.3) requires selecting a time window, which we fix at two weeks. Future work could extend this time window. If data are included for a longer window before the onset of the fire, a temporally-weighted regression could be used to emphasize recent observations. Compared to the standard spatial linear regression, the SL methods require the additional step of fitting several base learners. However, having established this procedure, the extra computing time is not prohibitive for making, say, daily or weekly risk predictions. Therefore, we believe the added flexibility of the SL approach justifies the additional computational burden.

In summary, our mixed-model approach offers a compelling alternative to single learners, physics-based simulators, empirical models, and statistical models to predict wildland burn severity in California. By leveraging the spatial SL method, researchers can achieve accurate predictions of burn severity and better our understanding of the drivers of burn severity which is needed for pre-fire season monitoring. Identifying the most important variables to be mindful of, such as evening soil moisture, can informs Californians of ways to effectively allocate their time and resources to prepare for and respond to wildland fire incidences. In doing so, the loss of human life, property, resources, and ecosystems could be minimized.

Appendix A.1: training individual learners

Part of the Super Learner algorithm is choosing the library of base learning models. These models were chosen to include a range of linear and non-linear methods. Specifically, the set comprised of Elastic Net, Decision Tree, Ridge regression, Lasso regression, K-Nearest neighbors, Gradient Boosting, Extreme



Table 11 Specifications for scikit-learn base learner model

Base learner	Hyperparameters
Ridge reg	Alpha = 1
Lasso reg	Alpha = 1
K neighbors reg	n_neighbors=6, weights="distance"
Gradient boosting reg	n_estimators=100, learn- ing_rate=0.1, max_depth=10, random_state=42
XGBoost reg	n_estimators=100, learn- ing_rate=0.1, max_depth=20, random_state=42
Bagging reg	n_estimators=100
Random forest reg	n_estimators=100
Extra trees reg	n_estimators=100

All other models use the default settings

Gradient Boosting (XGBoost), Bagging, Random Forest, Extra Trees, and a custom-built Neural Network model. All these models were trained using their scikit-learn default hyperparameters, except where explicitly mentioned otherwise. Specific hyperparameters are summarized in Table 11. The Super Learner code is publicly available on our GitHub page (https://github.com/Nicholas-Simafranca/Super_Learner_Wild_Fire.git).

The Neural Network model was implemented in PyTorch, comprising four fully connected hidden layers. All hidden layers used a rectified linear unit (ReLU) activation function. The output layer was a single neuron as this is a regression task. The model was trained using a mean squared error loss function and the Adam optimizer (Kingma and Ba 2014). The number of training epochs was set to 200 with a batch size of 115 and a learning rate of 0.01.

To generate the the out-of-fold predictions, a 10-fold cross-validation was performed on the entire dataset. In each fold of this cross-validation, each base model was trained on 80 percent of the data, and predictions were generated on the remaining 20 percent. This process was repeated such that every sample in the dataset had an associated set of out-of-fold predictions, one from each base learner. The out-of-fold predictions from all the base learners were then stacked horizontally to form a new matrix of meta-features, denoted as the *Z* matrix, one for each base learner (Fig. 2). Along with these meta-features, dNBR and corresponding latitude and longitude were also stored. The process of generating out-of-fold predictions ensured that the base learners and the meta-model remained decoupled, preventing data leakage and ensuring robustness of the ensemble.

In addition to generating out-of-fold predictions, the base learners were also trained on the entire training dataset, and predictions were made on the same dataset to obtain a set of fitted values. These fitted values were used to calculate the training RMSE for each base learner. Each base learning is fast to train. For example, for the KNP fire, the CPU time ranges from 141 milliseconds for Ridge



Regressor to 8 min and 31 s for XGBoost. Each base learner must be fit several times in the cross validation routine.

Appendix A.2: fitting the spatial model

Once all base learners had been trained and their out-of-fold predictions had been generated, the meta-model is trained using the GpGp: Fast Gaussian Process Computing package in R (Guinness et al. 2021). This package supports spatial models, including our exponential isotropic covariance function, with many ways of increasing computational efficiency. It implements Vecchia's Gaussian approximation, which is one of the most efficient Gaussian process approximations (Guinness 2021). Furthermore, Guinness (2021) improves upon Vecchia's approximation in the package by implementing a Fisher scoring algorithm for efficient computing of the maximum likelihood estimation of parameters, β , ϕ , τ^2 , σ^2 . Fitting the model requires less than two minutes for any of the fires. It also uses Vecchia's Gaussian approximation to predict at new unsampled locations, a form of Kriging (Allard et al. 2021). This utilizes computing the inverse Cholesky factorization of the covariance matrix when finding the conditional expectation as described in Allard et al. (2021) and Katzfuss et al. (2020). In its prediction, the package also orders and groups observations based on spatial proximity, further decreasing computing time (Allard et al. 2021).

Acknowledgements This work was carried out as part of a Research Experience for Undergraduates (REU). The authors would like to thank the organizers of the 2023 North Carolina State University "Directed Research for Undergraduates in Mathematics and Statistics" (DRUMS) program for their support and guidance. Funding was provided by the National Science Foundation (Grant DMS-2051010) and the National Security Agency (Grant H98230-23-1-0009). This work was also partially supported by National Science Foundation grant DMS-2152887. In addition, this research was partially carried out at the Jet Propulsion Laboratory, California Institute of Technology, under a contract with the National Aeronautics and Space Administration (80NM0018D0004). The authors would like to thank these collaborators for their insight and resources. Furthermore, the authors acknowledge the Minnesota Supercomputing Institute (MSI) at the University of Minnesota for providing resources that contributed to the research results reported within this paper. Lastly, the authors would like to acknowledge the computing resources provided by North Carolina State University High Performance Computing Services Core Facility.

Author Contributions NS, BW, EO and SF conducted the statistical analysis and wrote the main manuscript text, BR and NG planned the statistical analysis and MJ and MPC prepared the data and intepreted the results. All authors reviewed the manuscript

Declarations

Conflict of interest The authors declare no competing interests.

References

Allard D, Clarotto L, Opitz T, Romary T (2021) Discussion on competition on spatial statistics for large datasets. J Agric, Biol, Environ Stat 26:604–611

Breiman L (1996) Bagging predictors. Mach Learn 24:123-140

Breiman L (2001) Random forests. Mach Learn 45:5–32



- van Breugel P, Friis I, Demissew S, Lillesø J-PB, Kindt R (2015) Current and future fire regimes and their influence on natural vegetation in Ethiopia. Ecosystems 19:369–386
- California Department of Forestry and Fire Protection (2023) Cal fire incidents. https://www.fire.ca.gov/incidents/
- Chen T, Guestrin C (2016) Xgboost: A scalable tree boosting system. In: Proceedings of the 22nd acm sigkdd international conference on knowledge discovery and data mining, pp 785–794
- Coen JL, Stavros EN, Fites-Kaufman JA (2018) Deconstructing the king megafire. Ecol Appl 28:1565–1580
- Coop J, Parks S, Stevens-Rumann C, Crausbay S, Higuera P, Hurteau M, Tepley A, Whitman E, Assal T, Collins B, Davis K, Dobrowski S, Falk D, Fornwalt P, Fulé P, Harvey B, Kane V, Littlefield C, Margolis E, Rodman K (2020) Wildfire-driven forest conversion in western North American landscapes. Bioscience 70:659–673
- Cover T, Hart P (1967) Nearest neighbor pattern classification. IEEE Trans Inf Theory 13:21-27
- Davies MM, van der Laan MJ (2016) Optimal spatial prediction using ensemble machine learning. Int J Biostat. https://doi.org/10.1515/ijb-2014-0060/html
- Dennison PE, Brewer SC, Arnold JD, Moritz MA (2014) Large wildfire trends in the western United states, 1984–2011. Geophys Res Lett 41:2928–2933
- Kingma DP, Ba J (2014). Adam: A method for stochastic optimization. https://arxiv.org/abs/1412.6980.
- Fayad I, Baghdadi N, Bailly J-S, Barbier N, Gond V, Héraul B, Haj ME, Fabre F, Perrin J (2016) Regional scale rain-forest height mapping using regression-kriging of spaceborne and airborne LiDAR Data: application on French Guiana. J Remote Sens 8:240
- Fisher JB, Lee B, Purdy AJ, Halverson GH, Dohlen MB, Cawse-Nicholson K, Wang A, Anderson RG, Aragon B, Arain MA et al (2020) Ecostress: Nasa's next generation mission to measure evapotranspiration from the international space station. Water Resour Res 56:e2019WR026058
- Fisher JB, Whittaker RJ, Malhi Y (2010) Et come home: potential evapotranspiration in geographical ecology. Glob Ecol Biogeogr 20:1–18
- Friedl M, Sulla-Menashe D (2022) MODIS/Terra+aqua land cover type yearly L3 Global 500m SIN Grid V061. NASA EOSDIS Land Processes Distributed Active Arch Center. https://doi.org/10.5067/ MODIS/MCD12Q1.061
- Friedman JH (2001) Greedy function approximation: a gradient boosting machine. Annals Stat 29:1189–1232
- Erten Gamze Erdogan, Mahmut Yavuz CVD (2022) Combination of machine learning and kriging for spatial estimation of geological attributes. Nat Resour Res 31:191–213
- Geurts P, Ernst D, Wehenkel L (2006) Extremely randomized trees. Mach Learn 63:3–42
- Guinness J, Katzfuss M, Fahmy Y (2021) Gpgp: Fast gaussian process computation using vecchia's approximation. The Comprehensive R Archive Network
- Guinness J (2021) Gaussian process learning via Fisher scoring of Vecchia's approximation. J Stat Comput 31:25
- Heaney A, Stowell JD, Liu JC, Basu R, Marlier M, Kinney P (2022) Impacts of fine particulate matter from wildfire smoke on respiratory and cardiovascular health in California. GeoHealth 6:e2021GH000578
- Hengl T, Nussbaum M, Wright MN, Heuvelink GB, Gräler B (2018) Random forest as a generic framework for predictive modeling of spatial and spatio-temporal variables. Peer J 6:e5518
- Hijmans R J (2023) Geographic data analysis and modeling [r package raster version 3.6-23]. https://cran.r-project.org/web/packages/raster/index.html
- Hodges JS, Reich BJ (2010) Adding spatially-correlated errors can mess up the fixed effect you love. Am Stat 64:325–334
- Hoerl AE, Kennard RW (1970) Ridge regression: applications to nonorthogonal problems. Technometrics 12:69–82
- Hoerl AE, Kennard RW (1970) Ridge regression: biased estimation for nonorthogonal problems. Technometrics 12:55–67
- Hoffman CM, Canfield J, Linn RR, Mell W, Sieg CH, Pimont F, Ziegler J (2015) Evaluating crown fire rate of spread predictions from physics-based models. Fire Technol 52:221–237
- Hook S, Hulley G (2019) ECOSTRESS Evapotranspiration PT-JPL Daily L3 Global 70 m V001. NASA EOSDIS Land Process Distribut Active Archive Center. https://doi.org/10.5067/ECOSTRESS/ ECO3ETPTJPL.001



- Hook S, Hulley G (2019) ECOSTRESS Evapotranspiration PT-JPL Daily L4 Global 70 m V001. NASA EOSDIS Land Processes Distributed Active Archive Center. https://doi.org/10.5067/ECOSTRESS/ ECO4ESIPTJPL.001
- Hook S, Hulley G (2019) ECOSTRESS land surface temperature and emissivity daily L2 Global 70 m V001. NASA EOSDIS Land Process Distribut Active Arch Center. https://doi.org/10.5067/ECOST RESS/ECO2LSTE.001
- Hook S, Hulley G (2019) ECOSTRESS Water Use Efficiency Daily L4 Global 70 m V001. NASA EOS-DIS Land Process Distribut Active Arch Center. https://doi.org/10.5067/ECOSTRESS/ECO4WUE. 001
- Huang Y, Jin Y, Schwartz MW, Thorne JH (2020) Intensified burn severity in California's northern coastal mountains by drier climatic condition. Environ Res Lett 15:104033
- Hultquist C, Chen G, Zhao K (2014) A comparison of gaussian process regression, random forests and support vector regression for burn severity assessment in diseased forests. Remote Sens Lett 5:723–732
- InciWeb (2022) Incident information system. https://inciweb.nwcg.gov/
- Jain P, Coogan SC, Subramanian SG, Crowley M, Taylor S, Flannigan MD (2020) A review of machine learning applications in wildfire science and management. Environ Rev 28:478–505
- Jensen D, Reager JT, Zajic B, Rousseau N, Rodell M, Hinkley E (2018) The sensitivity of US wildfire occurrence to pre-season soil moisture conditions across ecosystems. Environ Res Lett 13:014021
- Kane VR, Cansler CA, Povak NA, Kane JT, McGaughey RJ, Lutz JA, Churchill DJ, North MP (2015) Mixed severity fire effects within the rim fire: Relative importance of local climate, fire weather, topography, and forest structure. Forest Ecol Manag 358:62–79
- Kane VR, Cansler CA, Povak NA, Kane JT, McGaughey RJ, Lutz JA, Churchill DJ, North MP (2015b) Mixed severity fire effects within the Rim fire: relative importance of local climate, fire weather, topography, and forest structure. For Ecol Manage 358:62–79
- Katzfuss M, Guinness J, Gong W, Zilber D (2020) Vecchia approximations of Gaussian-process predictions. J Agric, Biol, Environ Stat 25:383–414
- Keeley JE (2009) Fire intensity, fire severity and burn severity: a brief review and suggested usage. Int J Wildland Fire 18:116
- Kim H (2022) Bayesian additive regression trees in spatial data analysis with sparse observations. J Stat Comput Simul 92:3275–3300
- Koike K, Matsuda S, Gu B (2001) Evaluation of interpolation accuracy of neural kriging with application to temperature-distribution analysis. Math Geol. https://doi.org/10.1023/A:1011084812324
- van der Laan M J, Polley E C, Hubbard A E (2007) Super Learner. U.C Berkeley Divison of Biostatistics Working Paper Series, Working Paper 222
- Li J, Heap AD, Potter A, Daniell JJ (2011) Application of machine learning methods to spatial interpolation of environmental variables'. Environ Model Softw 26:1647–1659
- Masek J, Ju J, Roger J, Skakun S, Vermote E, Claverie M, Dungan J, Yin Z, Freitag B, Justice C (2021a) HLS Operational Land Imager Surface Reflectance and TOA Brightness Daily Global 30m v2.0. NASA EOSDIS Land Processes Distributed Active Archive Center. https://doi.org/10.5067/HLS/ HLSL30.002
- Masek J, Ju J, Roger J, Skakun S, Vermote E, Claverie M, Dungan J, Yin Z, Freitag B, Justice C (2021b) HLS Sentinel-2 Multi-spectral Instrument Surface Reflectance Daily Global 30m v2.0. NASA EOS-DIS Land Processes Distributed Active Archive Center. https://doi.org/10.5067/HLS/HLSS30.002
- Morgan JN, Sonquist JA (1963) Problems in the analysis of survey data, and a proposal. J Am Stat Assoc 58:415–434
- Jpl NASA (2013) NASA Shuttle Radar Topography Mission Global 1 arc second. NASA EOSDIS Land Processes Distributed Active Archive Center. https://doi.org/10.5067/MEaSUREs/SRTM/SRTMG L1.003
- Okoli C (2023) ale: Interpretable Machine Learning and Statistical Inference with Accumulated Local Effects (ALE). https://CRAN.R-project.org/package=ale. R package version 0.1.0
- Pascolini-Cambell M, Lee C, Stavros N, Fisher JB (2021) ECOSTRESS reveals pre-fire vegetation controls on burn severity for Southern California wildfires of 2020. Glob Ecol Biogeogr 31:1976–1989
- Pedregosa F, Varoquaux G, Gramfort A, Michel V, Thirion B, Grisel O, Blondel M, Prettenhofer P, Weiss R, Dubourg V, Vanderplas J, Passos A, Cournapeau D, Brucher M, Perrot M, Duchesnay E (2011) Scikit-learn: machine learning in Python. J Mach Learn Res 12:2825–2830
- PRISM Climate Group (2023) PRISM Climate Group. https://prism.oregonstate.edu/



Rosenblatt F (1958) The perceptron: a probabilistic model for information storage and organization in the brain. Psychol Rev 65:386

Saha A, Basu S, Datta A (2021) Random forests for spatially dependent data. J Am Stat Assoc 118:665–683

SMAP (2023) NASA Soil Moisture Active Passive. https://smap.jpl.nasa.gov/

Tibshirani R (1996) Regression shrinkage and selection via the lasso. J R Stat Soc Ser B Stat Methodol 58:267-288

Vecchia AV (1988) Estimation and model identification for continuous spatial processes. J Roy Stat Soc: Ser B (Methodol) 50:297–312

Wasser, L. (2019) Earth Analytics in R Course. https://qubeshub.org/publications/1439/1

Wikle CK, Zammit-Mangion A (2023) Statistical deep learning for spatial and spatiotemporal data. Stat Deep Learn Spatial Spatiotemporal Data. https://doi.org/10.1146/annurev-statistics-033021-112628

Yasrebi AB, Hezarkhani A, Afzal P, Karami R, Tehrani ME, Borumandnia A (2020) Application of an ordinary kriging-artificial neural network for elemental distribution in Kahang porphyry deposit Central Iran. Arabian J Geosci. https://doi.org/10.1007/s12517-020-05607-0

Zhou, Z.-H. (2021) Ensemble learning. SpringerLink

Zou H, Hastie T (2005) Regularization and variable selection via the elastic net. J R Stat Soc Ser B Stat Methodol 67:301–320

Springer Nature or its licensor (e.g. a society or other partner) holds exclusive rights to this article under a publishing agreement with the author(s) or other rightsholder(s); author self-archiving of the accepted manuscript version of this article is solely governed by the terms of such publishing agreement and applicable law.

Authors and Affiliations

Nicholas Simafranca¹ · Bryant Willoughby² · Erin O'Neil³ ·
Sophie Farr⁴ · Brian J. Reich² · Naomi Giertych² · Margaret C. Johnson⁵ ·
Madeleine A. Pascolini-Campbell⁵

- Brian J. Reich bjreich@ncsu.edu
- University of Minnesota Twin Cities, Minneapolis, USA
- North Carolina State University, Raleigh, USA
- University of California Los Angeles, Los Angeles, USA
- Vassar College, Poughkeepsie, USA
- Jet Propulsion Laboratory, California Institute of Technology, Pasadena, CA, USA

